Pharmaceutica Analytica Acta
ISSN: 2153-2435

Sangeetha et al., Pharm Anal Acta 2015, 6:6
DOI: 10.4172/2153-2435.1000385

Research Article Open Access

Crystal Growth, Structural Analysis, Characterization, Conformational Stability and Quantum Chemical Calculation of the Pharmaceutical Compound – P-Arsanilic Acid

Sangeetha M[1], Mathammal R[1]*, Mekala R[1] and Krishnakumar V[2]

[1]Department of Physics, Sri Sarada College for Women (Autonomous), Tamilnadu, India
[2]Department of Physics, Periyar university, Tamilnadu, India

Abstract

p-Arsanilic acid ,which is otherwise known as 4-amino phenyl arsonic acid, is a bioactive compound. Single crystals of p-Arsanilic acid (pAsA) are grown successfully under slow evaporation technique. The crystallinity and parameters of the grown crystal are determined with the powder x-ray diffraction result. The functional groups are characterized by FTIR and FT-RAMAN spectra. The UV spectrum reveals its application in the optoelectronic field. The molecular structure of the title compound is studied using density functional theory (DFT). The vibrational frequencies and the potential energy distribution (PED) are calculated using DFT/B3LYP 6-31+G** basis set. The stability of the molecule is determined by various conformers in the computational method. The HOMO-LUMO (Highest Occupied Molecular Orbital – Lowest Unoccupied Molecular Orbital) charge transfer and Non-Linear Optical (NLO) property determination were carried out. The electrophilic and nucleophilic attack of the molecule is studied using the MEP (Molecular Electrostatic Potential). The theoretical prediction of the thermodynamic properties helps in analysing the future application of the title compound.

Keywords: Characterization; Single crystal growth; Computer simulation; Arsanilic acid

Introduction

The physical properties of the solid state seen in crystals and powders of both drugs and pharmaceutical excipients are of interest because they can affect both the production of dosage forms and the performance of the finished product. The nature of the crystalline form of a drug may affect its stability in the solid state, its solution properties and its absorption. In order to study the stability and bioactivity of the title pharmaceutical compound, it is chosen for crystal growth and its properties are studied theoretically in detail.

The use of arsenic and its compounds are very popular in the production of pesticides, herbicides and insecticides. They are used as food additives in the poultry and swine industries in developing countries [1-3]. As a food additive, they control disease, simulate growth and improve both feed efficiency and conversion in animals. Majority of the organoarsenic compounds are not metabolized in the poultry and are excreted chemically unchanged and the manure is turned into fertilizer pellets for commercial use.

After the application of the fertilizer to soil, microbial activity and the presence of ultraviolet light lead to the formation of other organic arsenic species [4-6]. This in turn poses a number of health and environmental concerns. Since arsenic, in its various forms, is a known Carcinogen [7-11] it has been correlated with hypertension as well as other cardio metabolic diseases [12]. Arsanilic acid is used in the laboratory, for instance in recent modification of nanoparticles. It is also launched in chemotherapeutic approach for treating infectious diseases of humanbeings.

Density Functional Theory (DFT) is an effective cum economical tool for studying the structural properties of the molecule. Spectroscopic techniques eminently help in determining the dynamic behaviour of the electronic and molecular structures of natural products at microscopic level [13,14]. In this work, DFT technique is employed to study the complete vibrational spectra of p-Arsanilic acid.

Crystal Growth and Characterization Techniques

The pure sample of p-Arsanilic acid is purchased from Spectro. Chem Ltd, Mumbai, India and used as such for crystal growth. From the solubility test, sodium carbonate solution is found to be the good solvent. To the 50ml of sodium carbonate solution, the titled substance is dissolved up to the supersaturated state. Then the solution was filtered and kept undisturbed for slow evaporation. The nucleation began after 30 days. A single crystal of 20 x 10 x 5 mm^3 size was harvested at the seventh week. The transparency of the crystal is shown in Figure 1.

Figure 1: Grown crystal of p-Arsanilic acid.

***Corresponding author:** Mathammal R, Department of Physics, Sri Sarada College for Women (Autonomous), Salem-16, Tamilnadu, India, Tel: +91 427 2447664; E-mail: mathammals_shanmugam@yahoo.com

Received April 13, 2015; **Accepted** June 13, 2015; **Published** June 20, 2015

Citation: Sangeetha M, Mathammal R, Mekala R, Krishnakumar V (2015) Crystal Growth, Structural Analysis, Characterization, Conformational Stability and Quantum Chemical Calculation of the Pharmaceutical Compound – P-Arsanilic Acid. Pharm Anal Acta 6: 385. doi:10.4172/21532435.1000385

The grown crystal is subjected to powder x-ray diffraction studies to reveal the crystallinity of the substance. The powdered sample is scanned in the range 10-90° C at a scan rate of 2°/min using the JEOL JDX services instrument with CuKα (λ = 1.5406A˚) radiation. The room temperature FTIR spectrum of the title compound is measured in the region 4000-400 cm^{-1} with the scanning speed of 10 cm^{-1} min^{-1} and the spectral resolution of 4.0 cm^{-1} by employing Perking-Elmer spectrometer. The FT-Raman spectrum of the compound is recorded using Bruker FRA 106/S instrument equipped with Nd: YAG laser source operating at 1064 nm line widths with 100mW power. The spectrum is recorded in the range of 4000-10 cm^{-1}. ^{1}H and ^{13}C NMR (400 MHz; DMSO) spectra are recorded using BRUKER TPX-400 FT-NMR spectrometer. The optical absorption spectrum is recorded using Perkin-Elmer Lamda 935 UV-VIS-NIR spectrometer. The non- linear optical activity of the compound is determined using Kurtz powder technique.

Computational Details

Density functional theory (DFT) is extensively used due to their accuracy and low computational cost to calculate a wide variety of molecular properties and provided reliable results which were in accordance with experimental data. The molecular structure of pAsA and corresponding vibrational harmonic frequencies are calculated using Becke3-Lee-Yang-Parr (B3LYP) with 6-31+G** basis set using GAUSSIAN 09W [15] program package. No constraints are imposed on the structure during the geometry optimizations. The vibrational analyses, calculated at the same level of theory, indicate that the optimized structures are at the stationary points corresponding to local minima without any imaginary frequency.

Electronic properties: HOMO-LUMO energies, absorption wavelengths and oscillator strengths are calculated using B3LYP method, based on the optimized structure in gas phase. Thermodynamic properties of the title compound at different temperatures are calculated in gas phase. Moreover, the dipole moment, linear polarizabilities, hyperpolarizabilities and Mulliken atomic charge are also studied. The natural bonding orbital (NBO) calculations are performed using Gaussian 09 package at the same level in order to understand various second order interactions between the filled orbitals of one subsystem and vacant orbitals of another subsystem, which quantify the intermolecular delocalization or hyper conjugation. The second order perturbation theory analysis of Fock matrix in NBO basis of pAsA is carried out to evaluate the donor-acceptor interactions. The interactions result is a loss of occupancy from the localized NBO of the idealized Lewis structure into an empty non- Lewis orbital. 1H and 13C chemical shifts were calculated with GIAO approach [16] by applying B3LYP/6-31+G** method.

Results and Discussion

Powder X-Ray diffraction studies

The powder x-ray diffraction analysis helps in determining the crystalline nature of the grown crystal. Using the JEOL JDX services instrument with CuKα (λ = 1.5406A˚) radiation the sample is scanned with the range 10–90° C at a scan rate of 2° /min. The crystal belongs to monoclinic type and the lattice parameters obtained from the Powder XRD data are given below.

a = 7.241 (2)

b = 6.214(1)

c = 8.643 (1)

β = 101.19 (1)°

V= 381.5 (1) A^{o3}

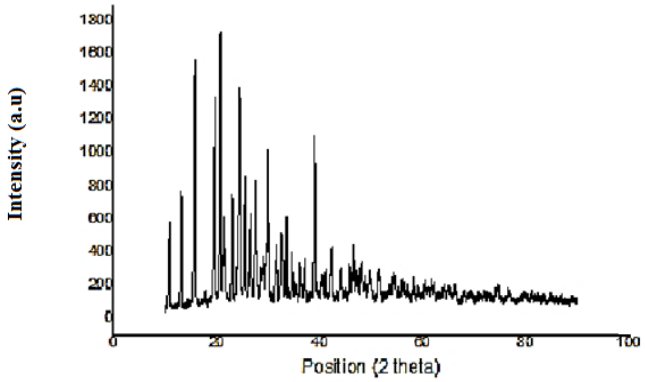

Figure 2: Powder X-ray diffraction pattern of pAsA crystals.

2θ	FWHM	d-spacing [A°]
10.857	0.281	8.142
13.125	0.221	6.740
19.597	0.191	4.5262
22.988	0.258	3.8657
24.511	0.15	3.629
29.54	0.49	3.022
32.574	0.23	2.7467
35.03	0.17	2.559
39.017	0.273	2.3067
44.03	0.35	2.0551
46.529	0.3	1.9627

Table 1: X-ray powder diffraction data of pAsA crystals.

The crystallinity of pAsA is well defined by the prominent peaks at specific 2θ values which can be seen in Figure 2. The d-spacing and their relative intensities of the diffraction peaks are tabulated in Table 1.

Conformational stability and molecular geometry

In order to determine the most stable structure of p-AsA, the energies of various conformers were calculated. The optimization was performed for the most stable conformer with global minimum energy. The conformers with their energy values are shown in Figure 3.

The molecular geometry of the title compound is described on the basis of bond lengths, bond angles and dihedral angles. The optimized parameters are tabulated in Table 2. The compound under investigation belong to C_1 point group symmetry with the global minimum energy E=-2747.732 Hartree. The optimized structure reveals that pAsA to be zwitter ionic form and it is shown in Figure 3a. The C-C bond length for pAsA calculated at B3LYP/6-31+G** level lies in the range 1.3883 to 1.4106 A^0. This coincides with the analogous molecule whose C-C bond length varies from 1.358 to 1.491 A^0 [17]. The presence of electronegative arsenic atom has reduced the calculated C-N bond length and it slightly varies from the experimental value (1.47 A^0) [18]. The substitution of arsenic in the ring exerts a valence electron cloud of nitrogen atom resulting in an increase force constant and decrease in bond length. The bond length between carbon and arsenic is probably large due to the electronegative nature of the arsenic. The As14-O15 and As14-O17 bond lengths, have the values 1.7702 and 1.7825 A^0, which coincides with the analogous molecule respectively [19]. The As14-O19 bond distance is reduced to 1.63 A^0 because of the inductive effect of the amino group. The O15-H16 bond and O17-H18 bond takes the value 0.9699 and 0.9705 A^0 respectively, which coincide with the analogous molecule [20].

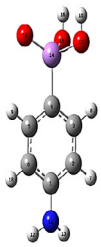

E = 2747.66823817Hartrees

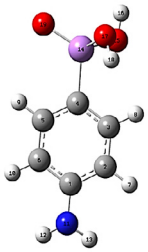

E = -2747.66112146 Hartrees

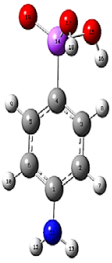

E = -2747.73297903 Hartrees

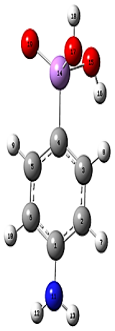

E = -2747.56643593 Hartrees

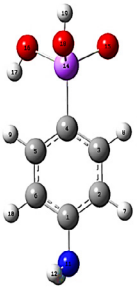

E= -2747.66281329 Hartrees

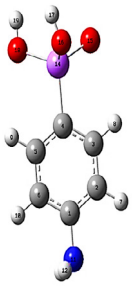

E = -2747.66457211 Hartrees

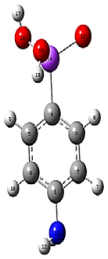

E = 2747.66161092 Hartrees

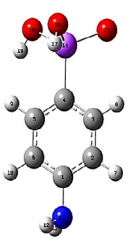

E = -2747.65560191 Hartrees

Figure 3: Various Conformers of p-Arsanilic acid.

The distortion in the ring is mainly due to the substituents and its consideration is very important. Among the six angles of ring, the angle C6-C1-C2 and C5-C4-C3 have a slight variation because of the presence of amine and arsenic group. The geometry optimization performed on the title compound indicates that it exhibits intramolecular hydrogen bond interaction. The magnitude of the bond angles O15-As14-O17 and O19-As14-O17 are 98.72° and 111.24° respectively, which indicates

Parameters	Theoretical	Parameters	Theoritical
Bond Length			
C1-C2	1.4106	As14-O15-H16	110.2084
C1-C6	1.4089	As14-O17-H18	107.6598
C1-N11	1.3843	Dihedral Angle	
C2-C3	1.3883	C6-C1-C2-C3	0.01
C2-H7	1.0868	C6-C1-C2-H7	179.7716
C3-C4	1.4013	N11-C1-C2-C3	-177.7358
C3-H8	1.0852	N11-C1-C2-H7	2.0257
C4-C5	1.4008	C2-C1-C6-C5	-0.0027
C4-As14	1.8917	C2-C1-C6-H10	-179.8692
C5-C6	1.39	N11-C1-C6-C5	177.7399
C5-H9	1.0859	N11-C1-C6-H10	-2.1265
C6-H10	1.0867	C2-C1-N11-H12	-162.6903
N11-H12	1.0093	C2-C1-N11-H13	-19.8578
N11-H13	1.0093	C6-C1-N11-H12	19.606
As14-O15	1.7702	C6-C1-N11-H13	162.4384
As14-O17	1.7825	C1-C2-C3-C4	-0.112
As14-O19	1.6363	C1-C2-C3-H8	-179.6999
O15-H16	0.9699	H7-C2-C3-C4	-179.873
O17-H18	0.9705	C2-C3-C4-C5	0.205
Bond Angle		C2-C3-C4-As14	179.585
C2-C1-C6	118.7955	H8-C3-C4-C5	179.7891
C2-C1-N11	120.5152	H8-C3-C4-As14	-0.8309
C6-C1-N11	120.6505	C3-C4-C5-C6	-0.1977
C1-C2-C3	120.49	C3-C4-C5-H9	-179.7452
C1-C2-H7	119.6407	As14-C4-C5-C6	-179.5954
C3-C2-H7	119.8688	As14-C4-C5-H9	0.857
C2-C3-C4	120.3845	C3-C4-As14-O15	48.8603
C2-C3-H8	119.3488	C3-C4-As14-O17	-54.3744
C4-C3-H8	120.2654	C3-C4-As14-O19	178.6839
C3-C4-C5	119.4813	C5-C4-As14-O15	-131.7558
C3-C4-As14	121.6775	C5-C4-As14-O17	125.0095
C5-C4-As14	118.8384	C5-C4-As14-O19	-1.9321
C4-C5-C6	120.4021	C4-C5-C6-C1	0.0974
C4-C5-H9	119.6425	C4-C5-C6-H10	179.9637
C6-C5-H9	119.9538	H9-C5-C6-C1	179.6436
C1-C6-C5	120.4463	H9-C5-C6-H10	-0.4901
C1-C6-H10	119.7126	C4-As14-O15-H16	-175.285
C5-C6-H10	119.841	O17-As14-O15-H16	-64.9221
C1-N11-H12	117.6733	O19-As14-O15-H16	54.5602
C1-N11-H13	117.7007	C4-As14-O17-H18	-114.98
H12-N11-H13	11.1385	015-As14-O17-H18	139.7087
C4-As14-O15	101.6574	O19-As14-O17-H18	15.7467
C4-As14-O17	107.8318	-	-
C4-As14-O19	117.906	-	-
O15-As14-O17	98.718	-	-
O15-As14-O19	117.371	-	-
O17-As14-O19	111.2429	-	-

Table 2: Optimized geometrical parameters of p-Arsanilic acid.

that As14-O17 is not symmetrically disposed on As14 and tilted towards O19 atom to form H-bonding between O19 and H18 atoms. The magnitude of the bond angles C1-N11-H12 and C1-N11-H13 is 117.6 and 117.70° respectively, which indicates that C1-N11 bond, is symmetrically disposed on C1.

Vibrational analysis

A complete vibrational assignment for the title compound is obtained using Gauss view program. The potential energy distribution (PED) illustrates the frequency distribution for the molecule under study. Most of the calculated frequencies are in coincidence with the available data. The optimized structure of pAsA comes under C_1 symmetry and has 51 normal modes of vibrations. The observed and calculated frequencies are summarised in the Table 3. The experimental and calculated FTIR spectra and FT-RAMAN spectra are shown in Figure 4 and 5.

Observed frequencies (in cm^{-1})		Calculated frequencies (in cm^{-1})		IR intensity	Raman intensity	PED(%)
		Unscaled frequencies	Scaled frequencies			
-	-	21	20	0.3095	3.3950	τHOAsC(92)
-	72	83	80	1.3174	3.2423	τring(44),δAsCCC(35), δOCOAs(15)
-	101	102	97	3.0357	0.9722	δAsCC(43),δOCOAs(20), βOAsO(11)
-	130	142	136	44.0230	1.9336	δOAsO(39),τHOAsC(36), βAsCC(11)
-	-	177	169	4.0025	0.2230	δOCOAs(26), τring(22)
-	192	228	218	21.8340	1.5824	τHOAsC(39), δOAsO(27)
-	241	233	223	23.5420	9.8303	vAsC(35),βOAsO(29)
-	-	282	269	25.0923	1.2246	δOCOAs(44),βOAsO(13),τHOAsC(11)
-	-	295	282	31.7708	1.5450	βOAsO(43), τHOAsC(24)
-	-	334	319	117.3647	2.8311	βOAsO(54), vAsC(13)
-	-	349	334	104.0826	1.3573	τHOAsC(28), δAsCCC(14)
-	-	352	337	54.6721	0.9138	δOCOAs(28) δAsCCC(14)
-	-	354	339	7.7920	0.1847	τHNCC(83)
-	362	406	388	0.2051	1.0149	βNCC(64), βAsCC(10)
-	401	435	416	330.4568	8.7377	βHNCC(83)
-	415	436	417	1.4405	0.0717	τring(79),τNCCC(10)
516	-	537	514	16.2490	0.5584	βring(54), τHOAsC(17)
610	-	619	592	2.7211	4.5056	βring(54), vAsC(23)
616	613	649	620	1.6575	5.4753	βring(79)
636	634	681	651	130.2023	24.6207	vAsO(93)
-	-	701	670	130.6002	15.7532	vAsO(94)
744	726	773	739	0.2750	0.1604	τring(48), τNCCC(22)
-	-	835	799	14.0495	25.8755	vCC(28), τHCCN(22), vCN(13)
-	808	838	801	2.1537	8.1850	τHCCN(63), τHCCC(11)
826	830	848	810	47.5682	3.2203	τHCCN(57), τHCCC(14)
-	-	971	928	41.1559	18.3490	vAsO(74) ,βHOAs(18)
		992	948	111.4965	1.9601	βHOAs(95)
975	-	1009	965	138.4029	1.9005	βHOAs(57), vAsO(19)
976	-	1014	970	7.0007	0.0720	τHCCC(51), τHCCN(20), τring(12)
-	-	1025	980	18.6809	7.2956	βHCC(40), vCC(22)
-	-	1037	992	0.5479	0.1766	τHCCC(56), τHCCN(20), τring(18)
1019	1012	1071	1024	0.4095	0.4537	βHNC(62), vCC(22)
1096	1094	1115	1066	75.6260	33.3023	vCC(49), vCAs(16)
-	-	1156	1105	3.5097	0.5701	βHCC(47), vCC(27)
1140	-	1215	1162	39.2371	5.9179	βHCC(72)
1234	-	1328	1269	101.4780	7.8833	vCN(51)
-	1289	1341	1282	10.4023	1.1439	vCC(39), βHCC(33)
1326	-	1372	1312	1.1265	0.3068	βHCC(24)vCC(23), βHCN(14)
1414	-	1465	1400	6.2808	0.2752	vCC(40), βHCC(31)
1474	-	1545	1477	58.6103	3.1089	βHCC(53)
-	-	1613	1542	9.2024	1.2640	vCC(71)
1571	-	1647	1575	72.1447	49.1366	vCC(37), βHNH(20)
1602	1594	1670	1596	265.0262	48.4841	βHNH(68)
2820	-	3182	3042	11.7466	100.3993	vCH(91)
2905	2993	3183	3043	11.7947	91.5474	vCH(98)
3033	3061	3206	3065	4.7684	86.0142	vCH(99)
-	3150	3210	3069	3.5663	102.8208	vCH(92)
3405	-	3595	3437	52.4562	263.5943	vNH(100)
-	3482	3709	3506	26.5557	64.5784	vNH(100)
-	3603	3799	3633	101.1245	89.7011	vOH(99)
-	-	3805	3638	99.7559	227.7897	vOH(99)

v – Stretching, β – bending, δ –out of plane, τ – torsion, PED- Potential Energy Distribution.

Table 3: Observed and B3LYP/6-31+G**level calculated vibrational frequencies (in cm^{-1}) of p-Arsanilic acid.

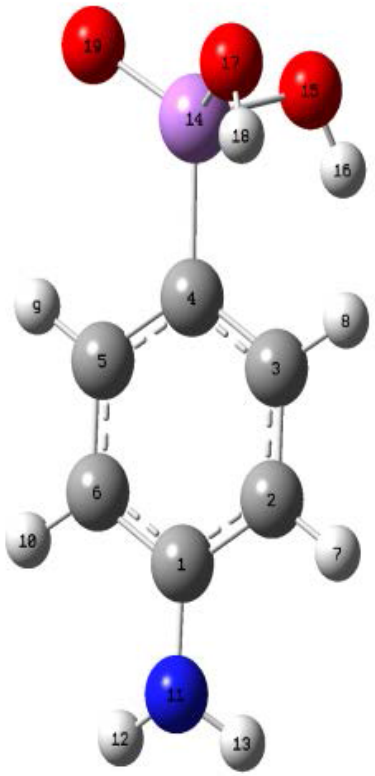

Figure 3a: Optimised structure of p-AsA with atom numbering.

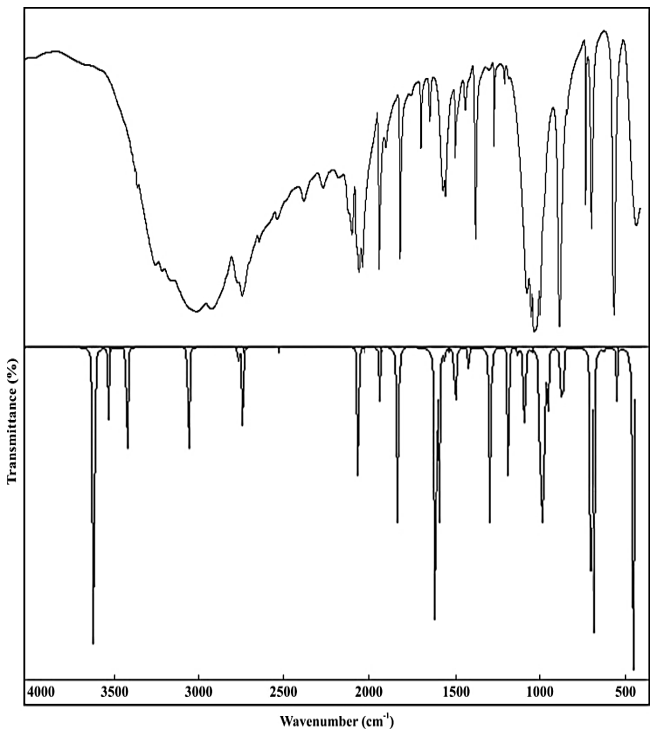

Figure 4: Comparison of observed and B3LYP/6-31+G** calculated FTIR spectra of p-Arsanilic acid.

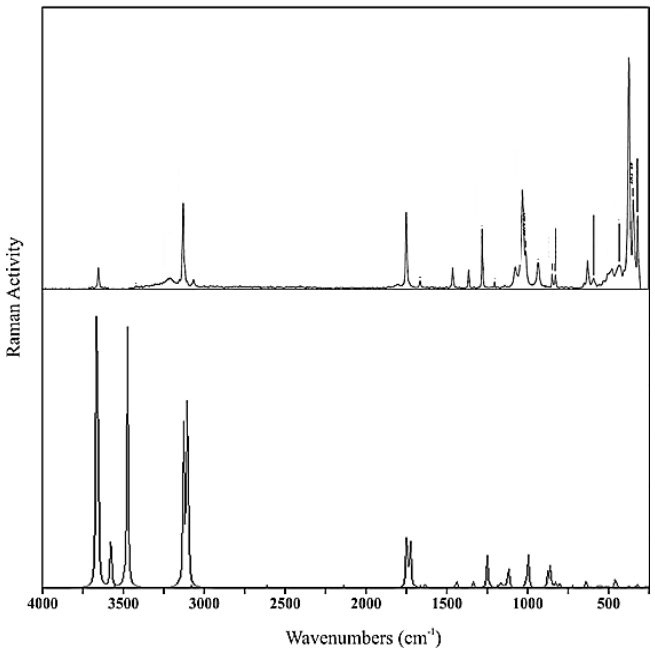

Figure 5: Comparison of Observed and B3LYP/6 -31+G** Calculated FT-RAMAN spectra of p-Arsanilic acid.

C-C vibrations: Generally, the C-C stretching vibration occurs in the region 1625-1430 cm^{-1}. The actual position of these modes is determined not so much by the form of substituents but by the form of substitution around the ring [21].The bands at 1571 cm^{-1}, 1414 cm^{-1}, 1289 cm^{-1}, 1096 cm^{-1} in the IR and 1289 cm^{-1}, 1094 cm^{-1} in Raman are assigned for CC stretching. The corresponding calculated frequencies take the values 1575, 1542, 1400, 1282, 1066 cm^{-1}. In aromatic ring, some bands are below 700 cm^{-1}. These bands are quite sensitive to change in nature and position of the substituents [22-25]. The in-plane vibration is at higher frequency than the out-of-plane vibration, which is due to the substituent group. The ring vibrations are observed at 516, 610, 616 cm^{-1} in IR, 614 cm^{-1} in Raman and their corresponding calculated frequencies are 514, 592 and 620 cm^{-1}. The ring torsional deformation vibrations are predicted at 726, 415 and 72 cm^{-1}, which are active in Raman.

C-H vibrations: The aromatic C-H stretching vibrations are normally found between 3100 and 3000 cm^{-1}. In this region, the bands are not affected appreciably by the nature of the substituents. The CH stretching mode is assigned to the peak at 2802, 2905 and 3033 cm^{-1} in the IR and the Raman active modes are at 2993, 3061 and 3150 cm^{-1}.The calculated frequencies at 3069,3065 and 3042 cm^{-1} also depict the CH stretching vibrations.

The region 1300-1000 cm^{-1} is expected for CH in-plane bending vibrations. Similarly for the title molecule the bands at 1326 and 1140 cm^{-1} are allotted for in-plane bending in IR spectrum. The CH out - of - plane vibrations is expected in the range 1000-700 cm^{-1}. For this molecule, the peak at 976 cm^{-1} is assigned for out –of –plane bending vibration and the calculated frequencies are 970 and 990 cm^{-1}.

As-O vibrations: The As-O stretching and bending vibrations are expected to appear in the region 1000-300 cm^{-1} [26]. However, the calculated band located at 928 cm^{-1} is assigned to the stretching mode of As-O band. The bond distance of As-OH types are 1.78 and 1.77A°. The greatest distance corresponds to the lowest wavenumbers at 670 and 651

cm^{-1}. The bands due to symmetric and asymmetric bending vibrations are identified in the 550-400 cm^{-1} frequency region in IR spectra. Two bands located at 319 and 282 cm^{-1} are assigned to asymmetric bending mode, whereas the symmetric mode appears at 136 cm^{-1}.

O-H and N-H vibrations: In dilute solutions, O-H stretching appears as a sharp band at higher frequency around 3600 cm^{-1} due to free O-H group. In spectra of undiluted liquids or solids, intermolecular hydrogen bonding broadens the band and shifts its position to lower frequency (3200–3500 cm^{-1})[27]. The peak at 3603 cm^{-1} in Raman is assigned to O-H stretching and the calculated frequency also falls at 3633 cm^{-1} with 100% PED contribution. The OH bending vibrations are observed in the region 965 and 948 cm^{-1} which coincides with the experimental data.

It is stated that in amines, the N-H stretching vibrations occur in the range 3400-3300 cm^{-1} [28]. With reference to this, the vibrational frequencies observed at 3482 in Raman and 3405 in IR are assigned to NH stretching modes. The peak observed at 1234 cm^{-1} is allotted for C-NH_2 stretching mode. The in-plane –NH_2 bending vibration falls from 1650-1580 cm^{-1}. The IR peak at 1602 cm^{-1} and Raman peak at 1594cm^{-1} is allotted for NH_2 bending vibration. Likewise, the out- of-plane bending -NH_2 band at 826 cm^{-1} in the IR 830 cm^{-1} in Raman is assigned to the amino group deformation mode.

NMR analysis

NMR serves as a great resource in determining the structure of an organic compound by revealing the hydrogen and carbon skeleton. Chemical shifts of pAsA are determined experimentally and the theoretical chemical shifts are predicted using Gauge – Invariant Atomic Orbitals (GIAO). The ^1H atom is mostly localized on periphery of the molecules and their chemical shifts would be more susceptible to inter molecular interactions in the aqueous solutions as compared to that of other heavier atoms. The chemical shift (δ) value provides information on the magnetic/chemical environment of the protons. Protons next to electron withdrawing groups are deshielded, whereas protons next to electron-donating groups are shielded [29].The experimental and calculated ^{13}C and ^1H NMR chemical shifts of the title molecule are gathered in Table 4. The hydrogen atoms attached to the electron withdrawing oxygen atom in the hydroxyl group decrease the shielding. This results in the low chemical shift for the hydroxyl protons. Whereas, the protons attached to the ring are in the range 6.87 - 8.04 ppm and the experimental values also fall in the same range coinciding with the theoretical data. Usually aromatic carbons possess the chemical shift values from 100 -150 ppm. Due to the influence of electronegative nitrogen atom, the chemical shift value of C1 of pAsA is significantly differing in the shift position and the corresponding value is 151.08 ppm. The experimental and calculated NMR spectra of ^1H and ^{13}C are shown in Figures 6 and 7.

C Atoms	Experimental Value	Theoretical Value	H Atoms	Experimental Value	Theoretical value
C1	151.08	136.806	H9	7.41	8.0449
C5	131.66	120.513	H8	7.39	7.9839
C3	131.38	118.83	H10	6.584	6.9026
C4	123.20	107.623	H7	6.563	6.8766
C2	113.05	100.052	H12	3.886	3.9084
C6	113.05	98.8976	H13	2.496	3.8931
-	-	-	H16	2.500	2.9492
-	-	-	H18	2.505	2.8436

Table 4: Experimental and Theoretical isotropic chemical shifts of p-Arsanilic acid.

Frontier molecular orbitals

The analysis of the wave function indicates that the electron absorption corresponds to a transition from the ground state to the excited state and is mainly described by one electron excitation from the HOMO to LUMO. Both HOMO and LUMO are the main orbital taking part in chemical reaction. HOMO energy characterizes the capability of electron giving; LUMO characterizes the capability of electron accepting [30]. The frontier orbital gap helps to characterize the chemical reactivity, optical polarizability, chemical hardness and softness of a molecule [31]. The surfaces for the frontier orbital are drawn to understand the bonding scheme of the title compound. Two important molecular orbital (MO) were examined for the title compound, the highest occupied molecular orbital (HOMO) and the lowest unoccupied molecular orbital (LUMO) are given in Figure 8. The calculated HOMO and LUMO energies are -0.23498eV and

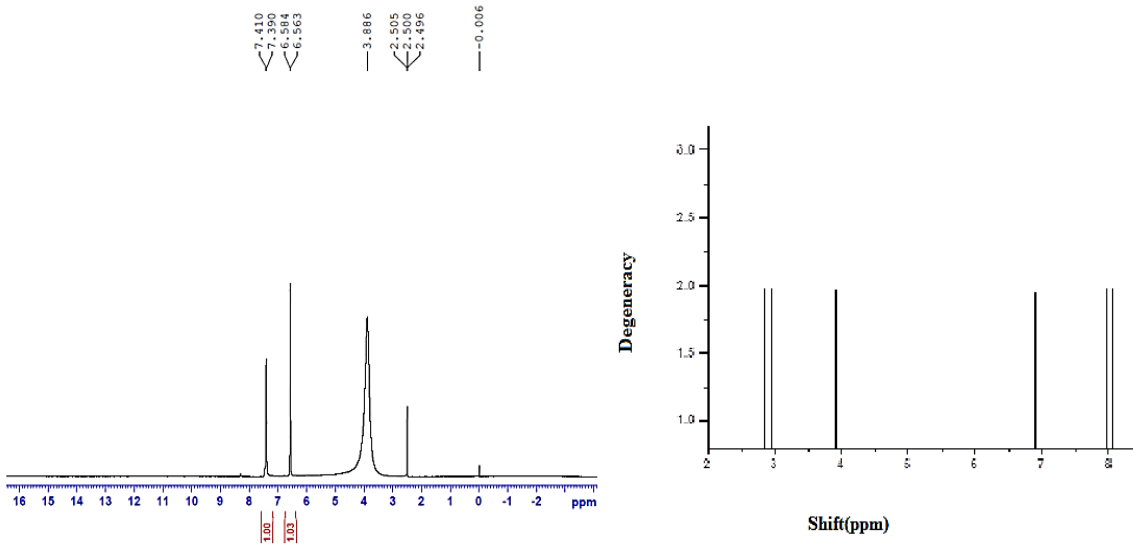

Figure 6:Experimental and Calculted ^1H NMR Spectrum of pAsA.

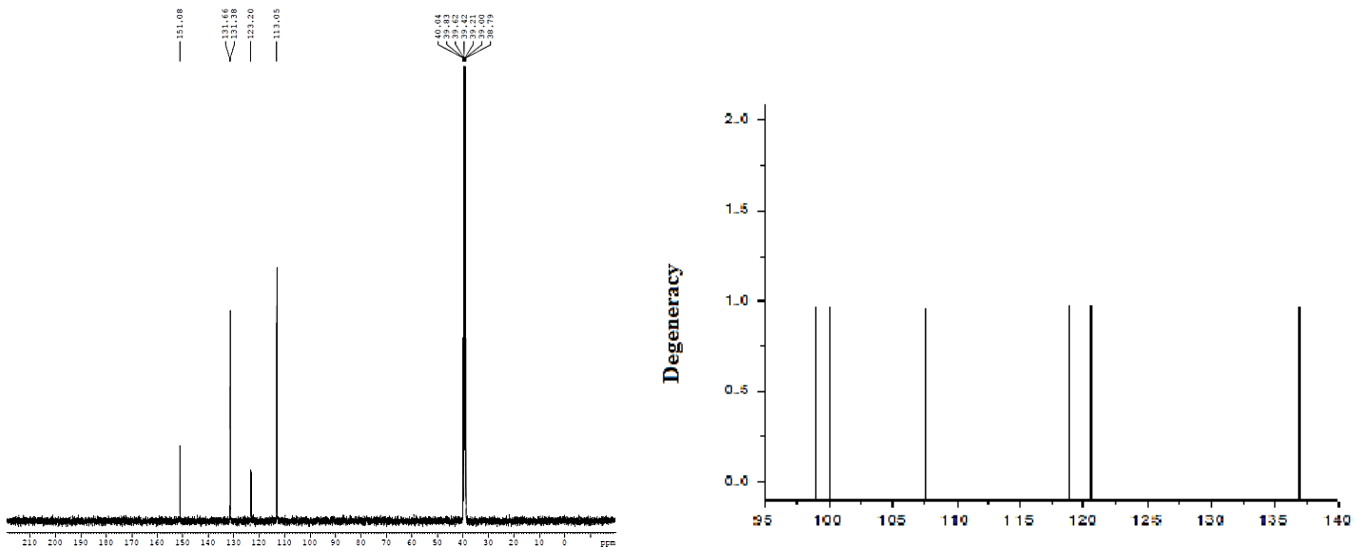

Figure 7: Experimental and Calculted ^{13}C NMR Spectrum of pAsA.

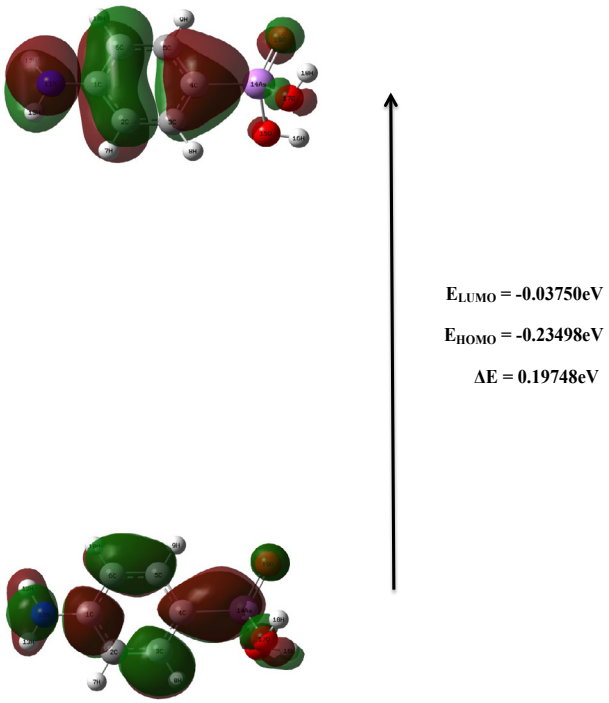

Figure 8 : The atomic orbital compositions of the frontier molecular orbital for p- Arsanilic acid.

-0.03750eV and the resulting band gap energy is 0.19748eV. The chemical stability of a molecule is determined by the hard and soft nature of it. HOMO-LUMO energy gap helps to find whether the molecule is hard or soft. Hard molecules have large energy gap and soft molecules have small energy gap. The soft molecules are more polarizable than the hard ones because they need small energy for excitation. The hardness value of a molecule can be determined as η = (-HOMO+LUMO)/2. The value of η of the title molecule is 0.13624eV. Hence, it shows that the title compound belongs to soft material.

NBO analysis

The NBO analysis is already proved to be an effective tool for the chemical interpretation of hyperconjugative interaction and electron density transfer from the filled lone pair electron [32]. In order to investigate the various second - order interaction between the filled orbitals of one subsystem and vacant orbitals of another subsystem the DFT/B3LYP level has been used, and it predicts the delocalization or hyperconjugation[33]. The hyperconjugative interaction energy can be deduced from the second-order perturbation approach [34]:

$$E^{(2)} = \Delta E_{ij} = q_j F(i,j)^2/\varepsilon_j - \varepsilon_i$$

Where q_j is the ith donor orbital occupancy, ε_j , ε_i are diagonal elements(orbital energies) and F(i,j) is the off-diagonal NBO Fock matrix elements.

The intramolecular interactions are formed by the orbital overlap between bonding (C-C), (C-As) and (As-O) antibonding orbital which results in the intra molecular charge transfer (ICT) causing stabilization of the system. These interactions are observed as increase in electron density(ED) in C-As, As-O antibonding orbital that weakens the respective bonds. A large number of stabilizing orbital interactions are calculated in pAsA and they are listed in Table 5.

The strong intra-molecular hyper-conjugative interaction of LP(2) O15→ σ*(As14-O19) increases the electron density ED(0.051e) that weakens the bonds leading to stabilization of 6.13 kcal/mol. Also the strong intra-molecular hyper-conjugative interaction of LP (2) O15→ σ*(As14-O17) weakens the respective bonds leading to stabilization 7.68 kcal/mol. Another strong intra – molecular hyper- conjugative interactions of C1-C6 from LP (1) N11 → π*C1-C6 increases ED (0.095e) that weakens the respective bonds leading to stabilization of 32.32 kcal/mol. These interactions are observed as an increase in electron density(ED) in C-C antibonding orbital that weakens the respective bonds. The increased electron density at the carbon atom leads to the elongation of respective bond length and a lowering of the corresponding stretching wave number.

Donor(I)	Types of Bond	Occupancy	Acceptor(J)	Types of Bond	Occupancy	E(2) Kcal/Mol	E(i)-E(j)a.u	F(i,j)
C1-C6	π	1.60800	C2-C3	π*	0.30266	14.39	0.28	0.058
		1.60800	C4-C5	π*	0.41175	28.92	0.27	0.079
C2-C3	π	1.71091	C1-C6	π*	0.40060	22.67	0.28	0.073
		1.71091	C4-C5	π*	0.41175	14.29	0.27	0.057
C4-C5	π	1.69512	C1-C6	π*	0.40060	13.69	0.28	0.057
		1.69512	C2-C3	π*	0.30266	23.73	0.29	0.074
C4-As14	σ	1.93366	As14-O15	σ*	0.20270	6.85	0.69	0.064
		1.93366	As14-O17	σ*	0.21155	7.80	0.69	0.068
		1.93366	As14-O19	σ*	0.09141	7.32	0.79	0.069
As14-O17	σ	1.96936	As14-O15	σ*	0.20270	6.60	0.80	0.068
As14-O19	σ	1.95966	As14-O17	σ*	0.21155	7.51	0.86	0.075
LPN11		1.81804	C1-C6	π*	0.40060	32.32	0.31	0.095
LPO15		1.94078	As14-O17	σ*	0.21155	7.68	0.42	0.053
			As14-O19	σ*	0.09141	6.13	0.52	0.051
LPO19		1.85321	C4-As14	σ*	0.13448	13.73	0.44	0.069
		1.85321	As14-O17	σ*	0.21155	12.40	0.34	0.059
LPO19		1.82500	As14-O15	σ*	0.20270	22.09	0.34	0.078
		1.82500	As14-O19	σ*	0.21155	13.48	0.34	0.061
	π*	0.41175	C2-C3	π*	0.30266	230.77	0.01	0.078
C4-As14	σ*	0.13448	As14-O19	σ*	0.09141	41.40	0.01	0.059

Table 5: The second-order perturbation energies E (2) (kcal/mol) corresponding to the most important charge transfer interactions (donor-acceptor) in pAsA by B3LYP/6-31+G** method.

UV-Vis spectra analysis

The grown crystal is subjected to UV-Vis-NIR spectral analysis and the lower cut-off wavelength is found to be 240nm. The wide transparency region in the visible and NIR region proves the molecule to be a good one for optical applications. The absorbance peak of the UV-Vis-NIR spectra is shown in Figure 9. Energy gap of pAsA is calculated by using the formula given below.

$$E = \frac{1.243 \times 10^{3}}{\lambda_{max}}$$ [35]

Where, λ is the lower cutoff wavelength and the energy gap value is found as 5.1375 eV.

Time-dependent density functional theory (TD-DFT) calculation is performed for pAsA on the basis of fully optimized ground state structure to investigate the electronic absorption properties. The λ_{max} values which are the function of electron availability, electronic excitation energies and oscillator strength are obtained from the UV-Visible spectra, simulated theoretically with B3LYP/6-31+G** basis set. The experimental and calculated visible absorption maxima are tabulated in Table 6. The theoretically predicted UV-Vis spectra are visualized in Figure 9, as can be seen from Table 6, the calculated absorption maxima values for pAsA have been found to be 267.96, 263.03 and 260.36nm. The oscillator strength for 260.36 nm is of higher in magnitude compared to other transitions. The absorption band of pAsA at the longer wave length region 267.96nm is caused by the n – π* transition.

Molecular electrostatic potential

The molecular electrostatic potential (MEP) is used primarily for predicting sites and relative reactivities towards electrophilic attack, in studies of biological recognition and hydrogen bonding interactions [36]. To predict the reactive sites for electrophilic and nucleophilic attack for pAsA, the MEP at the B3LYP/6-31+G** method is calculated as shown in Figure 10. Different colours on the MEP represent the different values of the electrostatic surface. The electrostatic potential increases in the order red<orange<yellow<green<blue. The colour code of the maps is in the range between -4.056eV (deepest red) and 4.506eV (deepest blue) in the title molecule, where blue colour indicates the strongest attractions and red indicates strongest repulsion. The region of negative V(r) is associated with the lone pair of electrons.

As seen from the Figure 10, in the pAsA the amine group region has negative potential and As-OH region has positive potential. The predominance of the light green region of MEPs surface corresponds to a potential halfway between the two extremes red and dark blue colour. The positive (blue) region of MEP is related to electrophilic reactivity and the negative (red) regions to nucleophilic reactivity.

Mulliken population analysis

The calculated Mulliken charges and natural charges of pAsA are listed in Table 7. The Mulliken analysis is the most common population analysis method. Mulliken atomic charge calculation has a significant role in the application of quantum chemical calculations to molecular systems because the atomic charges affect some properties of molecular system including dipole moment and molecular polarizability.

Excited state	Wavelengthλ(nm) Experimental	Theoretical	Excitation energy(eV)	Oscillator strength(f)
S1	240.19	267.96	4.6270	0.1442
S2	-	263.03	4.7137	0.0074
S3	-	260.36	4.7620	0.6156

Table 6: Experimental and Theoretical electronic absorption spectra values of p-Arsanilic acid using TD-DFT/B3LYP/6-31+G**.

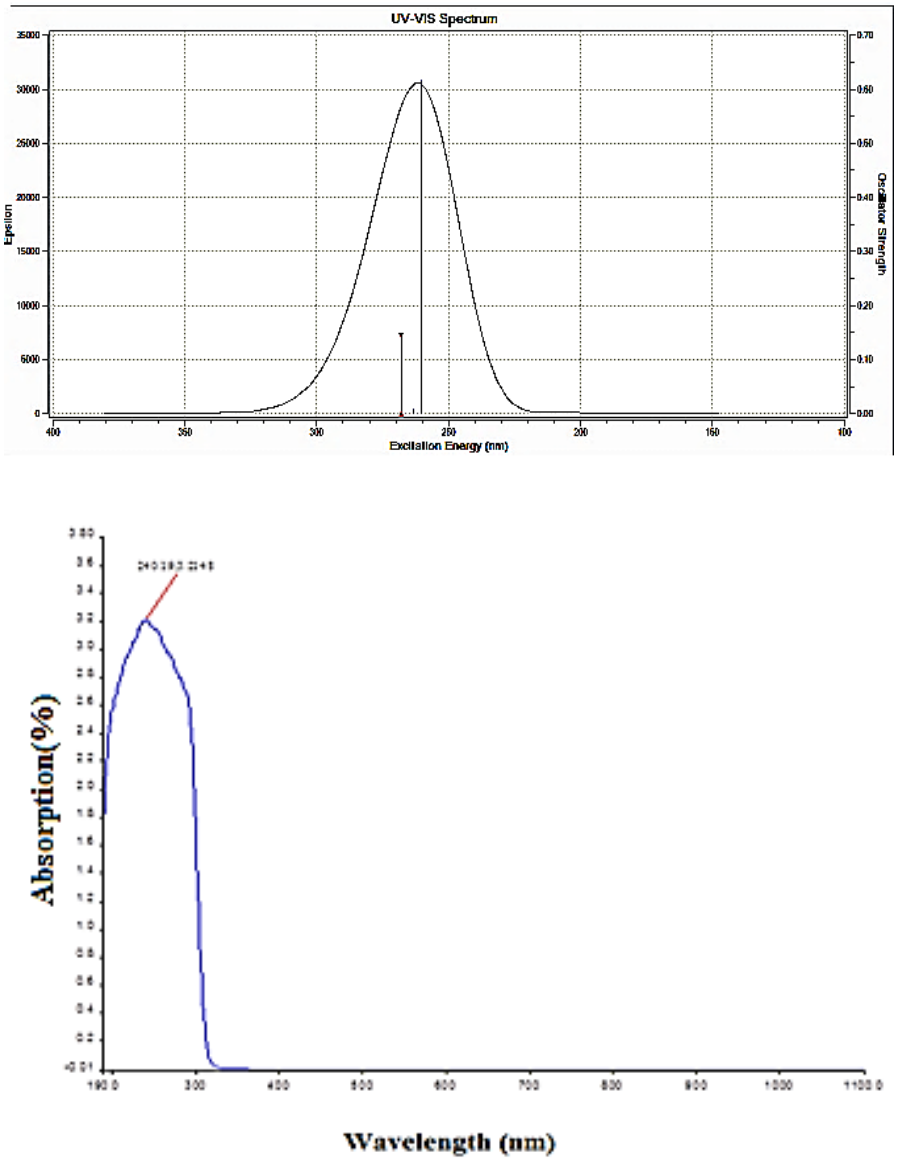

Figure 9 : Theoretically calculated and experimental UV-Vis spectrum of p-Arsanilic acid.

The obtained atomic charges for H7, H8, and H9 are smaller than the charges for H12 and H13, which is due to the presence of electronegative oxygen atom. In addition, the results illustrate that the charge of the oxygen atoms exhibits a negative charge, which are donor atoms. The results also show that the hydrogen atoms H16 and H17 have more positive atomic charge than the other hydrogen atoms. This is due to the presence of electronegative oxygen atom O17 and O19; the hydrogen atoms attract the positive charge from the oxygen atom.

NLO studies

In order to confirm the enhancement of nonlinearity of pAsA, second harmonic efficiency test is performed by the modified version of powder technique developed by Kurtz and Perry [37,38]. The powdered sample of pAsA crystal is illuminated using the fundamental beam of 1064nm from Q-switched ND:YAG laser. The input pulse energy of 1.9 mJ/pulse and pulse width 8 ns and repetition rate of 10 Hz are used. The second harmonic signal generated by the crystal was confirmed from the emission of green radiation of wavelength 532nm. The output voltage was 41mV and it was 0.5 times greater than the KDP value (76 mV).

In order to investigate the relationships between molecular structures and non-linear optical properties(NLO) , the polarizibilities and first order hyperpolarizabilities of the pAsA compound are calculated using DFT/B3LYP method with 6-31+G** basis set, based on finite field approach.

The polarizability and hyperpolarizability tensors can be obtained by a frequency job output file of Gaussian. The mean polarizability(α_{tot}), anisotropy of polarizability($\Delta\alpha$) and the average value of the first order hyperpolarizaility(β_{tot}) can be calculated using the equations

$$\alpha_{tot} = \alpha_{xx} + \alpha_{yy} + \alpha_{zz} / 3$$

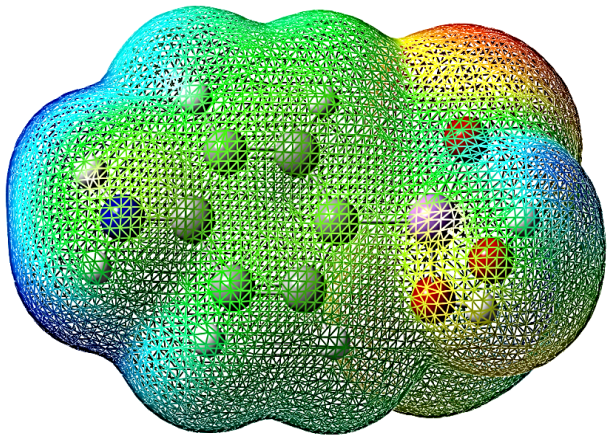

Figure 10: The total electron density isosurface mapped with molecular electrostatic potential of p-Arsanilic acid.

Atoms	Mulliken charges	Atomic charges
C1	-0.123	0.701
C2	0.423	-0.238
C3	-0.333	0.130
C4	-0.512	-0.478
C5	-0.467	0.128
C6	0.436	-0.236
H7	0.117	0.021
H8	0.144	0.062
H9	0.162	0.079
H10	0.118	0.023
N11	-0.589	-0.797
H12	0.295	0.207
H13	0.294	0.207
As14	1.144	2.244
O15	-0.589	-0.863
H16	0.370	0.284
O17	-0.610	-0.874
H18	0.366	0.278
O19	-0.647	-0.879

Table 7: Mulliken and Atomic charges of pAsA.

$$\Delta\alpha = 1/\sqrt{2}[(\alpha_{xx} - \alpha_{yy})^2 + (\alpha_{yy} - \alpha_{zz})^2 + (\alpha_{zz} - \alpha_{xx})^2 + 6\alpha^2_{xx}]^{1/2}$$

$$\beta = [(\beta_{xxx} + \beta_{xyy} + \beta_{xzz})^2 + (\beta_{yyy} + \beta_{yzz} + \beta_{yxx})^2 + (\beta_{zzz} + \beta_{zxx} + \beta_{zyy})^2]^{1/2}$$

The polarizability and hyperpolarizability are reported in atomic units(a.u), the calculated values have been converted into electrostatic units (esu) (for α : 1 a.u = 0.1482 x 10^{-24})esu, for β:1 a.u = 8.6393 x 10^{-33}) esu.

The total dipole moment (μ) for the title compound can be calculated using the following equation.

$$\mu = (\mu_x^2 + \mu_y^2 + \mu_z^2)^{1/2}$$

Theoretically calculated values of polarizability, first order hyperpolarizability and dipole moment are shown in Table 8. It is well-known that the higher value of dipole moment, molecular polarizability and first order hyperpolarizability are important for more active NLO properties. The large value of hyperpolarizability, β which is a function of the non-linear optical activity of the molecular system is associated with the intra molecular charge transfer. The

Parameters	B3LYP/6-31G(d,p)
α_{xx}	128.2024
α_{xy}	24.2041
α_{yy}	155.8194
α_{xz}	2.1473
α_{yz}	-1.5916
α_{zz}	77.8992
$\alpha_{tot\ (esu)}$	1.78788 X 10^{-23}esu
β_{xxx}	30.1831
β_{xxy}	188.5593
β_{xyy}	385.1353
β_{yyy}	441.4975
β_{xxz}	-17.8771
β_{xyz}	-17.9602
β_{yyz}	-6.9665
β_{xzz}	-21.2118
β_{yzz}	-22.5177
β_{zzz}	6.6632
$\beta_{tot(esu)}$	6.258 X 10^{-30}esu
μ_x	-0.4435721
μ_y	-1.9297488
μ_z	0.0928694
μ	1.98224

Table 8: The average polarizability (β_{tot}), first order hyperpolarizability(β_{tot}) and dipolemoment (μ) value of pAsA.

T (K)	$C^0_{p,m}$ (cal $mol^{-1}K^{-1}$)	ΔH^0_m (K cal mol^{-1})	S^0_m (cal $mol^{-1}K^{-1}$)
100	18.770	88.361	74.752
200	32.675	90.957	93.573
298.15	44.301	94.747	109.630
400	54.523	99.798	124.713
500	62.505	105.666	138.217
600	68.735	112.240	150.549
700	73.660	119.369	161.835
800	77.658	126.941	172.206
900	80.987	134.878	181.784
1000	83.813	143.122	190.676

Table 9: The temperature dependence of thermodynamic parameters of p-Arsanilic acid.

physical properties of these conjugated molecules are governed by the high degree of electronic charge delocalization along with the charge transfer axis and by the low band gaps. The calculated first order hyperpolarizability of the title compound is 6.258 X 10^{-30}esu, which is 48 times greater than that of urea (0.13 x 10^{-30} esu) [39]. So, it is revealed that the title molecule is an attractive object for future studies of non-linear optical properties.

Thermodynamic properties

The zero point energies, thermal correction to internal energy, enthalpy, Gibbs free energy and entropy and heat capacity for a molecular system are computed from the frequency calculations. The computed thermodynamic parameters are listed in Table 9. The correlation of heat capacity at constant pressure (C_p), entropy(S) and enthalpy change ($\Delta H_{o\to T}$) with temperature are delineated in Figure 11. As the temperature is increased from 100 to 1000K, the thermodynamic parameters also increase linearly. Here, all the mentioned thermodynamic calculations are done in gas phase. As per the second law of thermodynamics in thermochemical field [40], these calculations can be used to compute the other thermodynamic energies and help to estimate the directions of chemical reactions.

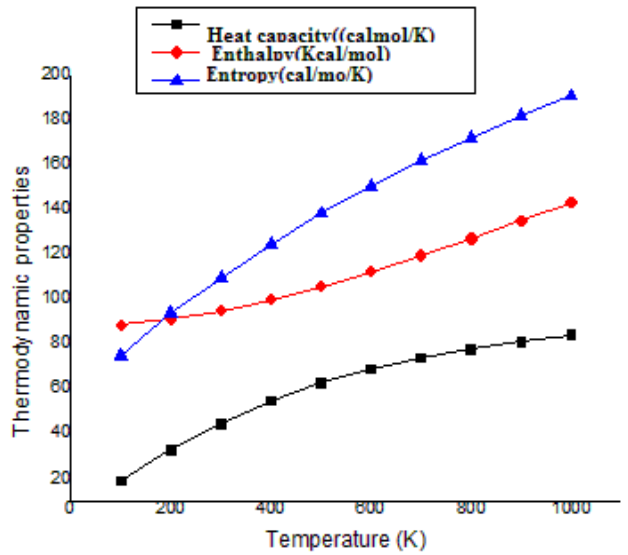

Figure 11: Temperature dependence of heat capacity, entropy and enthalpy change at constant pressure of p-AsA.

Conclusion

Single crystals of p-Arsanilic acid have been grown using the slow evaporation technique. The crystallinity and the cell parameters have been revealed by the powder XRD results. The detailed vibrational analysis has been studied using DFT/B3LYP method and most of the calculated frequencies coincide with the experimental FTIR and FT-RAMAN data. The UV studies show a wide transparency region above the lower cut-off region and large band gap energy. This proves the optical quality of the crystal. The emission of green radiation from the SHG studies is yet another proof for title compound to be a good NLO material. The stability, chemical reactivity, intramolecular interaction of the molecule are analysed with the help of theoretical calculations in detail. . The molecular electrostatic potential surface (ESP) provides information regarding the size, shape, charge density distribution and sites of chemical reactivity of the title molecule .The intermolecular interactions in the compound is found out with the help of the reactive sites. A deep insight into the charge transfer is elucidated by NBO analysis. The correlations between the thermodynamics and temperature are also obtained.

Acknowledgement

The authors are sincerely thankful to the SHG measurement facility extended by Prof.P.K.Das, Department of Inorganic and physical chemistry, Indian Institute of Science, Bangalore. The authors are also thankful to Sophisticated Analytical Instrumentation Facility (SAIF), IIT, Chennai, and St. Joseph's College, Trichirappalli, India for providing spectral measurements.

References

1. Jones FT (2007) A Broad View of Arsenic. Poult Sci 86: 2-14.
2. Cullen WR (2008) Is Arsenic an Aphrodisiac? The sociochemistry of an Element. RSC Publishing Cambridge.
3. Canadian Food Inspection Agency- Arsanilic acid (Date Revised 2006-09)
4. Cortinas I, Filed JA, Kopplin M, Garbarinco JR, Gandolfi AJ, et al. (2006) Anaerobic Biotransformation of Roxarsone and related N-Substituted Phenylarsonic acids. Environ. Sci.Technol 40: 2951-2957.
5. Markris KC, Quazi M, Pumamiya P, Sarkar D, Datta R (2008) Fate of Arsenic in Swine Waste from concentrated Animal feeding Operations. J.Environ.Qual 37:1626-1633.
6. Jackson BP, Bertsch PM (2001) Determination of Arsenic speciation in Poultry wastes by IC-ICP-MS. Environ.Sci.Technol 35: 4868-4873.
7. Bissena M, Frimmel FH (2003) Arsenic-a Review Part I: Occurrence, Toxicity, Speciation, Mobility. Acta Hydrochim, Hydrobiol 31: 9-18.
8. Dopp E, Hartmann LM, Florea AM, Rettenmeier AW, Hirner AV (2004) Environmental Distribution, Analysis, and Toxicity of organometal(Loid) Compounds. Critical Rev. Toxic 34: 301-333.
9. Kenyon EM (2001) A Concise Review of the Toxicity and Carcinogenicity of Dimethyl arsenic Acid. Toxicology 160: 227-236.
10. Tchounwou PB, Centeno JA, Patlolla AK (2004) Arsenic Toxicity, Mutagenesis, and Carcinogenesis- a Health Risk Assessment and Management Approach. Mol.Cell.Biochem 255: 47-55.
11. Hirano S, Kobayashi Y, Hayakawa T, Cui X, Yamamoto M, et al. (2005) Accumulation and Toxicity of Monophenyl Arsenicals in Rat Endothelial Cells. Arch. Toxicol 79: 54-61.
12. Abhyankar LN, Jones MR, Guallar E, Navas-Acien A (2012) Arsenic Exposure and Hypertension: A Systematic Review. Environ. Health Perspect 120: 494-500.
13. Srivastava P Tandon, Jain S, Asthana (2011) Spectrochim Acta A 84: 141-155.
14. Joshi BD, Srivastava A, Tandon P, Jain S (2011) Molecular structure, vibrational spectra and HOMO, LUMO analysis of yohimbine hydrochloride by density functional theory and ab initio Hartree–Fock calculations. Spectrochim.Acta A 82: 270-278.
15. Frisch MJ (2009) Gaussian 09, Revision A.1, Gaussian, Inc., Wallingford CT.
16. Wolinski K, Haacke R, Hinton JF, Pulay P (1997) J Comp Chem 18: 816-825.
17. Moreno- Fuquen R, doP.Gambardella MT, Santos RH (1997) Complex Formed by 2-Picoline N-Oxide and 3-Chlorobenzoic Acid. Acta Cryst C 52: 1635-1637
18. Moreno- Fuquen R, doP.Gambardella MT, Santos RH (1996) Complex Formed by 2-Picoline N-Oxide and 4-Nitrophenol. Acta Cryst C 52: 1745-1747.
19. Adamescu A, Hamilton I, Al-badleh HA (2014) Density functional theory calculations on the complexation of p-arsanilic acid with hydrated iron oxide clusters: structures, reaction energies, and transition states. J.Phys.Chem.A 118: 5667-79.
20. Bellamy LJ (1980) The Infrared Spectra of Complex Molecules (3rd edn) Wiley, New York.
21. Gupta RK, Prasad R, Bhatnagar HL (1990) Indian J Pure Appl Phys 28533.
22. Jakobsen RJ, Bentley FF (1964) Vibrational Spectra of Benzene Derivatives. II. Frequency Assignments in the CsBr Region. Appl. Spectrosc 18: 88-92.
23. Mansingh (1970) Far-Infrared Absorption in Ortho- and meta-Dihalobenzenes. J. Chem. Phys 52: 5896-5901.
24. Verdonck L, Kelen GPV, EeckhantZ (1973) Benzyl compounds—VII: The far infrared and Raman spectra of meta-substituted benzyl compounds Spectrochim. Acta A 29 (1973) 813-816.
25. Verdonck L, Kelen GPV (1972) Far infrared and Raman spectra of para-substituted benzyl derivatives Spectrochim. Acta A 28: 55-57.
26. Glenening ED, Reed AE, Carpenter JE, Weinhold F (1998) NBO Version 3.1. TCI, University of Wisconsin, Madison.
27. Kalsi PS (2007) Spectroscopy of Organic Compounds (6th edn) New Age International (P) Limited Publishers, New Delhi.
28. Ahmed AB, Feki H, Abid Y, Minot C (2010) Molecular structure, vibrational spectra and nonlinear optical properties of orthoarsenic acid–tris-(hydroxymethyl)-aminomethane DFT study. Spectrochimica Acta Part A. 75: 1315-1320.
29. K.Fukui K (1982) Role of Frontier Orbitals in Chemical Reactions Science 218: 747-754.
30. Kosar B, Albayrak C (2011) Spectroscopic investigations and quantum chemical computational study of (E)-4-methoxy-2-[(p-tolylimino) methyl]phenol Spectrochim. Acta 78A: 160-167.
31. Luque FJ, Lopez JM, Orozco M (2000) Perspective on "Electrostatic interactions of a solute with a continuum. A direct utilization of ab initio molecular potentials for the prevision of solvent effects" Theor. Chem.Acc. 103: 343-345.
32. Yang Y, Zhang W, Gao X (2006) Blue-shifted and red-shifted hydrogen bonds:

Theoretical study of the CH3CHO· · ·HNO complexes. Int.J.Quant.Chem 106: 1199-1207.

33. Chocholousova J, Vladimir Spirko V, Hobza P (2004) First local minimum of the formic acid dimer exhibits simultaneously red-shifted O–HO and improper blue-shifted C–HO hydrogen bonds. Phys. Chem. Chem.Phys 6: 37-41.

34. Jag Mohan (2001) Organic Spectroscopy Principles and Applications (2nd edn) New Age International(P) Limited Publishers, New Delhi.

35. Dillip GR, Raghavaiah P, Mallikarjuna K, Madhukar Reddy K, Bhagavannarayana G, et al. Crystal growth and characterization of γ-glycine grown from potassium fluoride for photonic applications. Spectrochimica Acta part A 79: 1123-1127.

36. Adant C, Durpuis M, Bredas JL (2004) Int J Quantum Chem 56: 497-507.

37. Kurtz SK, Perry TT (1968) A powder technique for the evaluation of nonlinear optical materials. J. Appl. Phys 39: 3798-3813.

38. Franken PA, Hill AE, Peters CW, Weinreich G (1961) Generation of optical harmonics. Phys. Rev. Lett 7: 118-119.

39. Adant C, Durpuis M , Bredas JL (2004) Ab initio study of the nonlinear optical properties of urea: Electron correlation and dispersion effects. Int.J.Quantum Chem 56: 497-507.

40. Sebastian S, Sylvestre S, Sundaraganesan N, Amalanathan M, Ayyapan S, et al. (2004) Vibrational spectra, molecular structure, natural bond orbital, first order hyperpolarizability, TD-DFT and thermodynamic analysis of 4-amino-3-hydroxy-1-naphthalenesulfonic acid by DFT approach Spectrochim. Acta. 107: 167-178.